Nuclear Engineering and Design 439 (2025) 114056

Contents lists available at ScienceDirect

Nuclear Engineering and Design

journal homepage: www.elsevier.com/locate/nucengdes

SMR core thermal hydraulic experiments and code validation with the MOTEL test facility

Heikki Suikkanen [a,*], Joonas Telkkä [a], Antti Räsänen [a], Eetu Kotro [a], Michael Böttcher [b], Lucia Rueda-Villegas [c], Veronika Sunkova [d]

[a] Nuclear Engineering, LUT School of Energy Systems, LUT University, Yliopistonkatu 34, Lappeenranta, 53850, Finland
[b] Institute for Neutron Physics and Reactor Technology, Karsruhe Institute of Technology, Hermann-von-Helmholtz-Platz 1, Eggenstein-Leopoldshafen, 76344, Germany
[c] Tractebel-Engie, Bld Simon Bolivar 36, Bruxelles, 1000, Belgium
[d] UJV Rez, a.s., Hlavní 130, Řež, Husinec, 25068, Czech Republic

ARTICLE INFO

Keywords:
Thermal-hydraulics
Experiments
CFD
Subchannel analysis
Validation
SMR

ABSTRACT

Thermal hydraulic experiments with the modular integral test facility, MOTEL, were performed as a part of the European McSAFER research project. The facility models an integral pressure water small modular reactor (SMR) with a helical steam generator and a core with separate heater rod groups, in which power can be individually controlled. Different asymmetric and ring-shaped radial core power distributions were imposed in the experiments to provoke cross flows in the buoyancy-driven coolant flow. The purpose of the experiments was to produce new SMR-relevant data for the validation of computational fluid dynamic (CFD) and thermal-hydraulic subchannel codes. The experimental measurements revealed cross flow mixing effects, mainly in the top part of the core. Obtaining visible differences in the fluid temperature measurements between different heater regions required significant power gradients between the regions. CFD simulations were performed using ANSYS CFX with a detailed model comprising the whole primary side of the facility, and additional investigations were conducted with a stand-alone model of the heat exchanger. Good agreement with the measurements was obtained with the CFD simulations, which also revealed further details of the core flow characteristics in an asymmetric heating case. Furthermore, simulations with the subchannel codes, CTF and VIPRE-01, were performed. The simulations with CTF highlighted the code's capability to handle flow rates typical to natural circulation driven SMRs, as the results agreed well with the experiments and were able to predict the correct axial temperature profiles in the different regions of the core. VIPRE-01 solution stability was found to be highly sensitive to the flow rate, the power level, and the axial nodalization. Simulations with VIPRE-01 ended unsuccessfully due to convergence issues, and it was concluded that the conditions of the experiments are beyond the current capabilities of the code.

1. Introduction

Small modular reactors (SMR) are visioned to complement traditional nuclear power reactors and variable renewables in future energy systems as versatile energy sources, producing electricity but also other commodities like district heat (Truong et al., 2021; Leppänen et al., 2021; Skoda et al., 2020), industrial heat (Peakman and Merk, 2019), desalinated water (Al-Othman et al., 2019), and hydrogen (Locatelli et al., 2018). The economic feasibility of SMRs relies mainly on the series production model, with modular construction and simplified systems that can be realized due to a significantly smaller power output than in typical operating power reactors today (Mignacca and Locatelli, 2020; Lloyd et al., 2021). The International Atomic Energy Agency (IAEA) lists over 80 different SMR designs, of which more than 30 are water cooled reactors (IAEA, 2022). Despite most of these water cooled designs represent well-known pressurized or boiling water reactor technology, they seek the above mentioned economic feasibility via unconventional design choices like integral primary circuit design, helical or plate heat exchangers, and natural circulation operation of safety systems, but in some designs also of the primary cooling. Yet, as for any nuclear reactor, the safety of an SMR needs to be demonstrated as a part of the licensing process. Computer codes are used for this purpose, but such codes need to be applicable to the purpose and capable to simulate the phenomena and processes of relevance, which

* Corresponding author.
E-mail address: heikki.suikkanen@lut.fi (H. Suikkanen).

https://doi.org/10.1016/j.nucengdes.2025.114056
Received 13 August 2024; Received in revised form 18 February 2025; Accepted 4 April 2025
Available online 23 April 2025

is conventionally demonstrated by comparing the simulations against measurements obtained from representative experiments carried out with separate effect or integral effect test facilities (IAEA, 2019). Considering the new design features in light water SMRs, the applicability of computational tools validated for traditional reactors cannot be taken for granted for SMRs and needs to be re-assessed.

One effort to produce SMR-relevant measurement data with experiments and perform code validation was recently realized within the European McSAFER project, which combined thermal hydraulic experiments and code validation for light water SMRs, in addition to the development and demonstration of multi-physics and multi-scale methods for SMR safety analyses (Sanchez-Espinoza et al., 2021). Three large scale test facilities were used to produce data from the fundamental heat transfer phenomena, such as critical heat flux, and the behaviour of novel components, such as helical steam generators, to the integral loop behaviour in both forced and natural circulation, as well as forced-to-natural circulation transients (Suikkanen et al., 2023). The data from the experiments was then used to validate various computational tools, including computational fluid dynamics (CFD), subchannel and system thermal hydraulic codes. This paper documents one set of McSAFER experiments and the related validation of subchannel and CFD codes against experiments conducted with the MOTEL (MOdular TEst Loop) test facility operated at LUT University in Lappeenranta, Finland (Hyvärinen et al., 2024). MOTEL is an integral test facility representing an integral pressure water reactor (iPWR) type SMR operating at natural circulation. Unlike more traditional loop-type PWRs, iPWRs contain all major primary circuit components inside a single pressure vessel. Previously, MOTEL was used in experiments focused on the behaviour of the helical coil steam generator, as documented by Telkkä et al. (2023).

In the work presented in this paper, MOTEL was used for core flow experiments, where the aim was to impose irregular radial power distributions that would drive cross flows in the core operated at natural circulation. This is possible as the facility features an electrically heated core composed of more than one hundred heated rods distributed in separate heating regions. The experiments were supported by a detailed CFD analysis, on one hand to validate the CFD simulation approach for this type of reactor analyses, and on the other hand to provide further insight to the flow behaviour in the core to complement the limited core instrumentation. The CFD analysis was performed at the Karlsruhe Institute of Technology in Germany. The data from the experiments was then used to assess the capabilities of different subchannel codes to simulate the low flow rate natural circulation flow together with radial heating irregularities. These simulations were attempted with the codes CTF at the Tractebel-Engie in Belgium and VIPRE-01 at the UJV Rez, a. s. in Czech Republic.

2. MOTEL test facility

MOTEL is a modular integral test facility operated by the Nuclear Engineering research group at LUT University. The facility consists of flange-connected modules that, in principle, facilitate possible modifications via flexible addition or replacement of components (Hyvärinen et al., 2017). This way, the facility can be configured to represent different reactor technologies. The current version of MOTEL represents an iPWR with some resemblance to the NuScale power module (Ingersoll et al., 2014) due to the adoption of a helical coil type steam generator (SG) and operation by natural circulation. However, MOTEL is not a scaled down version of the NuScale power module but a more generic SMR model meant for studying thermal hydraulic phenomena rather than serving as an experimental validation of a specific reactor design.

The structure of the MOTEL facility is shown in Fig. 1. The main components, or modules, of MOTEL are the core module at the bottom, the SG module in the middle, and the pressurizer module at the top. In addition, a short extension piece connects the core and the SG modules to provide additional height between the heat source and the heat sink.

Table 1
Main dimensions and operating parameters of the MOTEL facility.

Parameter	Value
Total height	7400 mm
Outer diameter	711 mm
Core heated length	1830 mm
Diameter of heater and measurement rods	19.05 mm
Diameter of dummy rods	18 mm
SG tube outer diameter	15 mm
SG total heat transfer area	17 m^2
Max primary/secondary pressure	4 MPa
Max primary/secondary temperature	250 °C
Max core heating power	990 kW

Together, the outer shells of these modules form the pressure vessel of the facility. Inside the vessel, in addition to the main components mentioned above, there is a riser pipe that extends from the bottom of the core to the top of the SG module. In the core module, the riser pipe with a diameter of 610 mm surrounds the core and forms an annular downcomer space, thus separating the upwards flowing core cooling flow from the downwards flowing return flow. Above the core, the riser pipe narrows down to a diameter of 485 mm so that the annulus space in the SG module is increased to accommodate the helical SG tubes. The water heated by the core rises through the riser pipe to the top of the heat exchanger module, turns around, and flows downwards through the annulus, releasing heat to the secondary side through the SG tubes. The secondary water flows in the tube side in a total of 16 tubes, and the SG is capable of producing superheated steam (Telkkä et al., 2023). After exiting the SG module, the cooled down primary flow falls to the bottom of the core module via the downcomer space before entering the core again.

In the secondary side, there is a feed water reservoir from which water is pumped to the SG. There are four cold collectors, each distributing the water to four tubes, such that the SG consists of 16 tubes in total. Similarly, the tubes connect to four hot collectors, from which pipelines lead the produced heat outside of the pressure vessel. The instrumentation of MOTEL is based on point-form temperature, pressure, and differential pressure measurements, as well as on traditional flow rate measurements in the secondary side and ultrasonic flow meters in the primary side. The MOTEL vessel is insulated mainly with 120 mm thick rock wool supported by a 1 mm thick aluminium alloy plate. Some parts with limited space, such as inlets for steam generator and some flanges, have a reduced insulation thickness of 50 mm. Heat losses of the facility have been quantified in earlier experiments and documented by Hyvärinen et al. (2022).

The main dimensions and maximum operating parameters of the MOTEL facility are presented in Table 1. As the work presented in this paper is focused on the core flow and heat transfer, the core design and instrumentation are discussed in more detail in Sections 2.1 and 2.2, respectively. More general information about the facility and especially of the steam generator is given by Telkkä et al. (2023).

2.1. Core design

The core consists of 132 electrically heated heater rods, 145 unheated dummy rods, and 16 hollow instrument rods (see Fig. 2) that contain thermocouples for fluid temperature measurements. The rods are organized in a square lattice so that the heater and dummy rods alternate; every second rod being a heater rod, with some of the heated positions replaced by an instrument rod, as shown in Fig. 3 along with the relevant dimensions. The dummy rods are used to reduce the coolant space in the core to better model the coolant flow in a standard fuel rod assembly. Specifically, they create comparable friction to reproduce pressure losses within the core similar to SMR designs such as the NuScale power module.

The heater rods are distributed into 12 heater sections, for which the heating power can be individually controlled with solid state relays.

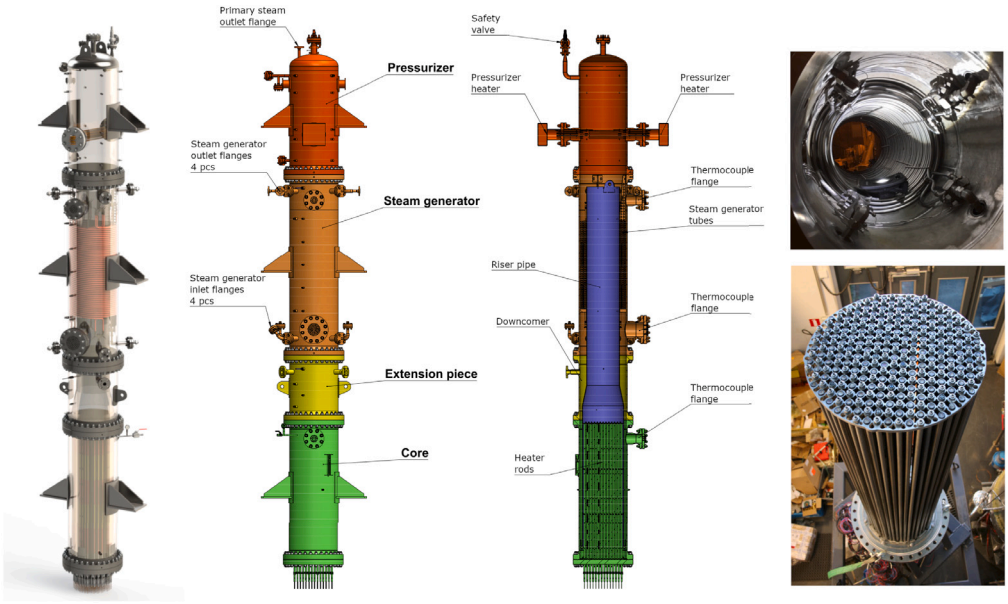

Fig. 1. A 3D model of the MOTEL test facility (left), the main modules and internal structure (middle), and photos of the steam generator tubes (top right) and the core rods (bottom right) taken during the assembly of the facility.

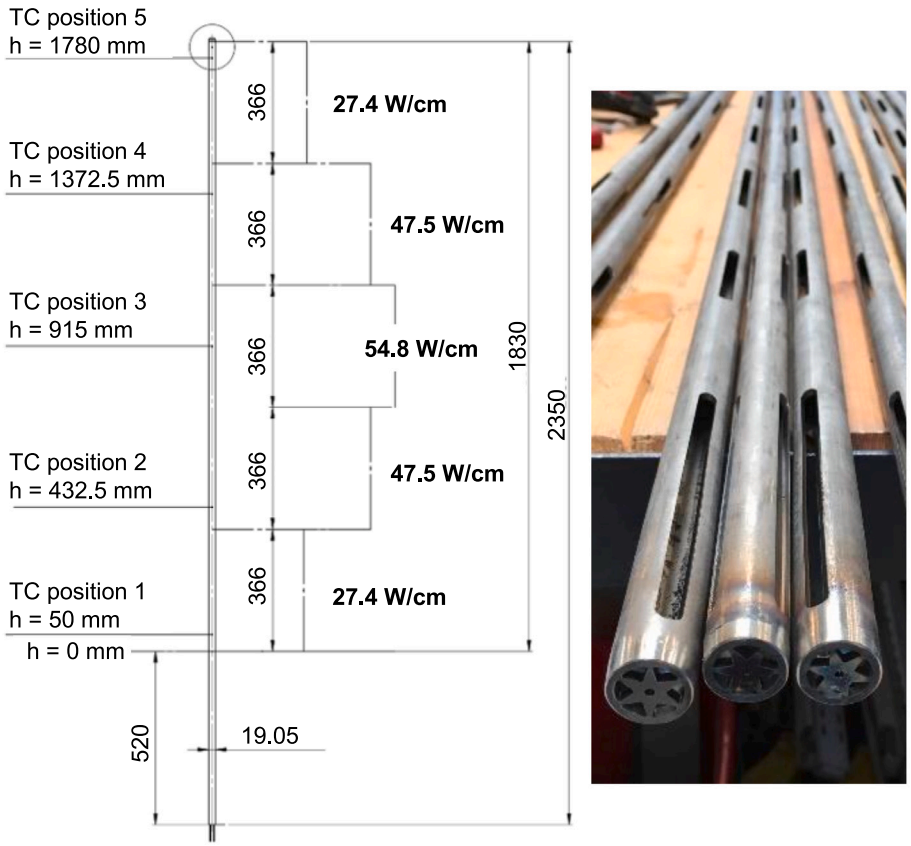

Fig. 2. The possible temperature measurement positions along the heated rod length, and the axial heating profile assuming the maximum rod heating power (left). Hollow instrument rods with crevices machined on the surface to facilitate fluid flow inside the rod, where thermocouples are installed (right).

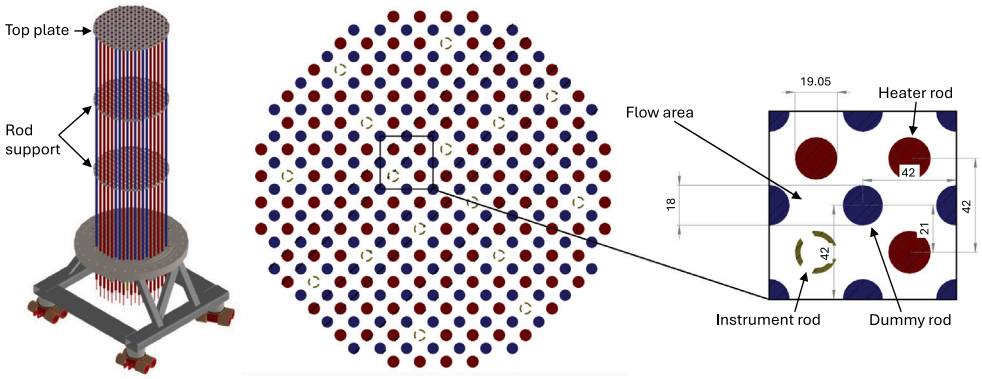

Fig. 3. A 3D model of the MOTEL core (left), and the rod arrangement (middle) with the heater rods in red colour, dummy rods in blue colour, and instrument rods as hollow. The core lattice dimensions (right) are in mm.

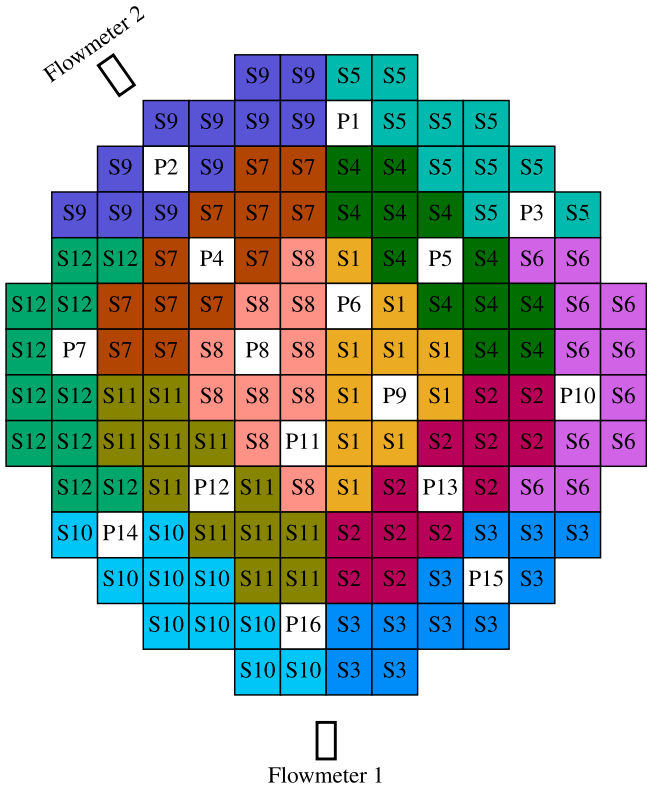

Fig. 4. Heater rod division into twelve sections (S1...S12), and instrument probe positions (P1...P16), with each square representing a single heater or instrument rod. The positions of the two flowmeters relative to the heater sections are also shown.

These heater sections are shown in Fig. 4. This feature makes it possible to perform experiments with different radial power distributions. Axially, the power distribution is fixed to a stepwise cosine shape, as shown in Fig. 2. The maximum heating power of a single heater rod is 7.5 kW, so the maximum total core power is 990 kW.

2.2. Core instrumentation

There is no optical access to the inside of the core module, which limits the types of measurement instruments that can be used to obtain data. The core instrumentation in MOTEL consists of J type thermocouples (iron constantan) inside the heater rods and K type thermocouples (NiCr-Ni) in the instrument rods. Each heater rod contains one thermocouple at one of the five positions defined in Fig. 2. These are installed inside the rod between the cladding and the magnesium oxide insulation. The instrument rods are intended to measure the fluid temperature, and these hollow rods each have thermocouples at the five positions specified in Fig. 2. The instrument rods are highly windowed, as shown in Fig. 2, and the thermocouples are located in these windowed locations. Thus, we expect them to provide a reasonable estimation of the coolant temperature between the heated rods.

The core inlet flow can be estimated based on two ultrasonic flowmeters that measure the mass flow rate in the bottom part of the downcomer. They are installed on the outer surface of the pressure vessel with a 145° angle between them, as shown in Fig. 4, thus not exactly on opposite sides of the facility to minimize the possible interference between the measurements.

3. Core thermal hydraulic experiments

Two sets of core experiments were defined, with the first one with radially asymmetric power distributions and the second one with ring-shaped power distributions. As a boundary condition for all distributions, the core total heating power was kept below 250 kW, which was also used in previous experiments by Telkkä et al. (2023) as the maximum heating power at which the steam generator behaviour was stable in the defined operating conditions, with the primary and secondary pressures at 2 MPa and 0.5 MPa, respectively. It should be noted that the tests were not intended to directly represent any reactor operation or safety analysis scenario but to provide challenging cases for the simulation tools. Also, it was anticipated that significant power gradients would be required to observe noticeable differences in the fluid temperature measurements across the core cross section.

3.1. Asymmetric power distributions

Four asymmetric power distributions were tested. In the first three, the core was divided radially into two halves with different heating powers, while keeping the core total power at 230 kW in each test. In the fourth asymmetric test, power was applied in only two heater sections (S9 and S7 in Fig. 4) using heating power close to the maximum of each rod, so that the total power was 170 kW. In all tests, the axial power distribution in the rods had the cosine shape shown in Fig. 2. The experiments were conducted as a single run, where the facility was first heated up using the heating power of 230 kW. In the beginning and in between the third and fourth tests, a reference run of 30 min in duration with a uniform power distribution using the total core power of the next test was performed.

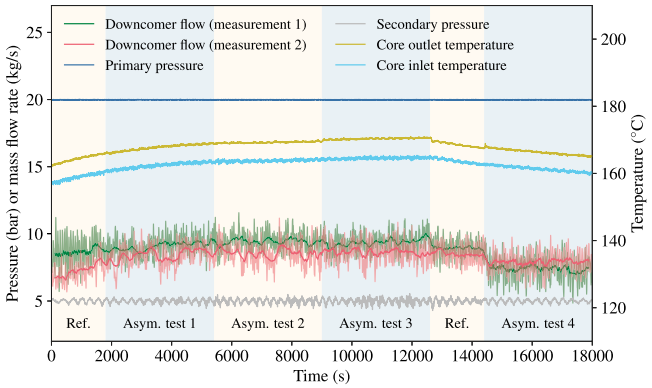

Fig. 5. Overview of the asymmetric experiments. For the downcomer flow, a moving average of the actual measured data is presented in darker shade.

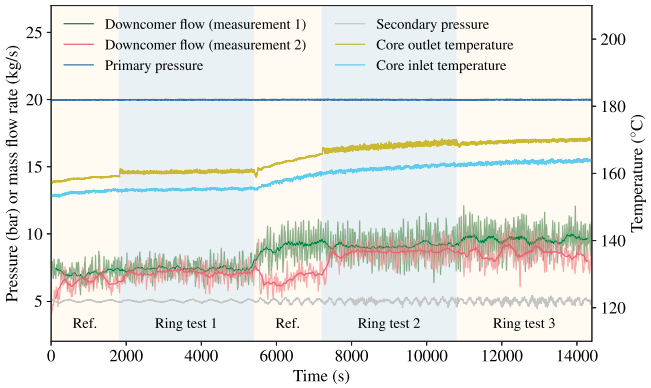

Fig. 6. Overview of the ring-shaped experiments. For the downcomer flow, a moving average of the actual measured data is presented in darker shade.

3.2. Ring-shaped power distributions

Three ring-shaped power distributions were tested. In these experiments, the core cross section was divided into three concentric areas, for which different heating powers were applied. In the first test, only the innermost area (S1 and S8 in Fig. 4) was heated with the total power of 150 kW, that is, using the maximum power the heater rods. This was done also in the second test, but additionally, heating power of 10% of the maximum was used in all the other rods, so that the total core power was 235 kW. The third test was performed with different heating powers in all the three concentric regions, such that the rods in the innermost, middle, and outer regions had heating powers of 52%, 31%, and 10% of the maximum, respectively. The total power in this case was 235 kW. Before the first test, a reference run of 30 min was performed with uniformly distributed heating at 150 kW total core power, and the same was done before the second test using 235 kW total power.

3.3. Experimental results

The overall progress of the asymmetric power distribution experiments is shown in Fig. 5. The downcomer flow, measured with two ultrasonic flowmeters at the bottom part of the vessel, more or less represents the core inlet flow. The measurements show significant noise, so also a moving average of the data is presented. The data reveals slightly lover flow rate measured by the second flowmeter, except in the Asymmetric test 4, in which the heated sections S7 and S9 coincide with the location of the second flow meter, and the first flowmeter is located in the unheated part of the core. There is no flowmeter positioned completely in the unheated/low-power half to measure what the possible difference in the inlet flow between the two halves is in the first three asymmetric tests. The best estimate is thus given by the comparison between Flowmeter 1, located at the border of the two halves, and Flowmeter 2, located in the hot half. Temperatures in Fig. 5 are measured at the bottom part of the downcomer, representing the core inlet temperature, and at the centre of the riser pipe just above the core, representing the core outlet temperature. These, as well as other measured temperatures, show slight gradients during the tests. There was limited time available to conduct the experiments in the laboratory. Thus, not fully steady states were achieved during the steps. Nevertheless, we consider the steps long enough for detecting temperature distributions inside the core.

The overall behaviour is similar for the experiments with the ring-shaped power distributions, as seen in Fig. 6. Again, a slightly lower flow rate is measured with the second flow meter; the difference between the measurements being smallest in Ring test 1 and largest in Ring test 3. The measured temperatures show slight increase during the tests, except in Ring test 1, which is closest to a steady state.

The axial fluid temperature distributions in the measurement probe positions are shown in Fig. 7 for the asymmetric heating tests and in Fig. 8 for the ring-shaped heating tests. The values at the axial measurement positions are obtained by taking a 1 min average of the temperature measurements at the end of each test. For compactness, Asymmetric test 1 is not presented as it shows practically identical behaviour as Asymmetric test 2. In general, it can be noticed that significant heating power gradients are needed for obtaining noticeable differences in the measured fluid temperatures across the core cross section. As can be seen in Figs. 7(a) and 8(c), where the differences in heater powers between the different heated regions are small, the radial distribution of the coolant temperature remains rather uniform across the core. Temperature differences arise when the heating power gradient between the regions is increased. Asymmetric test 3, shown in Fig. 7(b), seems to represent a threshold case where the thermocouples located deep in the hot region measure slightly higher temperatures than the other thermocouples up to the midway of the core but, then the warmer and colder flows mix toward the top of the core and result in a relatively uniform temperature distribution across the cross section at the core outlet. When the heating power difference between regions is further increased, as in Asymmetric test 4 (Fig. 7(c)) and Ring tests 1 and 2 (Fig. 8(a) and (b)), the hot region temperatures clearly depart from the cold region with increasing difference towards the top of the core. Some evidence of the mixing of flows between the hot and cold regions can be seen when looking at the measurements located at the boundary of the hot and cold region, which show temperatures slightly departing from the other measurements located deeper in the cold region. This is most visible in Asymmetric test 4 (Fig. 7(c)), which also shows, together with Ring test 1 (Fig. 8(a)), the largest spread of 4...5 °C in the measured temperatures across the core cross section at the top of the core. It should be noted, however, that the measurement uncertainty for the fluid temperature measurements is ±2 °C.

4. CFD analysis

A model of the MOTEL primary side was developed for a CFD analysis with ANSYS CFX. This type of simulations are computationally demanding due to the selected detailed CFD approach described in Section 4.1. For this reason, the CFD analysis focused on a single asymmetric heating power case. Asymmetric test 3 (see Fig. 5) was selected, where half of the core heater sections are heated for a time interval of about 1 h, with powers indicated in Fig. 7(b). For a Reynolds-averaged Navier–Stokes (RANS) steady state analysis, the time interval between 10000 s and 11000 s was chosen. The measured data of the core power distribution was averaged for the selected time frame and used as a heat flux boundary condition for the core heater rods.

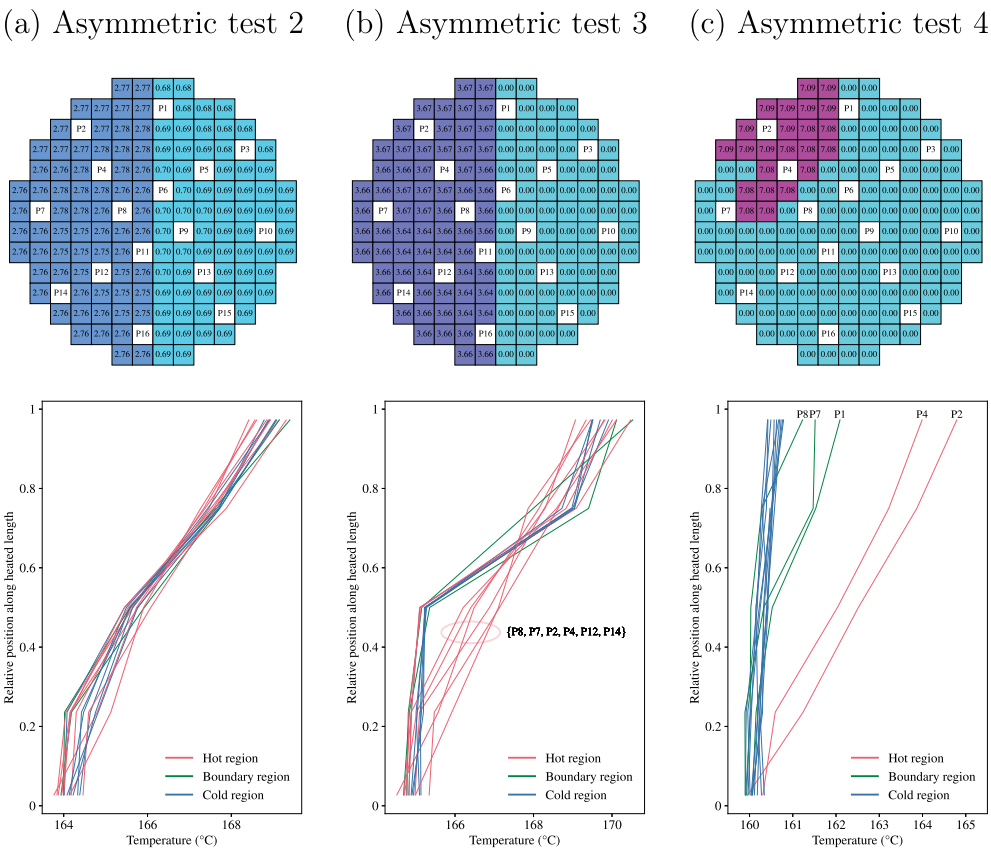

Fig. 7. Axial fluid temperature profiles measured with the instrument probes in three asymmetric heating power tests. The curves are coloured based on their location, either in the region with the highest heating power (Hot region), the unheated or lower heating power region (Cold region), or in the cold region but right next to the hot region (Boundary region). The applied power distribution in each test is displayed above, with the numbers being the power of each heater rod in kW.

4.1. CFD model description

The challenges for the CFD model are the complex geometry with heat transfer in coolant and solid, combined with buoyancy driven flow, as there are no pumps to drive the coolant in the primary side. The use of porous media regions are mostly combined with the specification of pressure loss coefficients, which becomes inaccurate at low velocities, as given in this case. The selected scenario deals with asymmetric core heating, so that the entire vessel has to be modelled in detail and handled as a closed system, because core induced asymmetric velocity distributions propagate through the entire primary system.

Fig. 9 shows the CFD model with meshing details in the core and the SG region. All vessel internals, which are causing relevant pressure loss, are resolved by the mesh, such as core rods, spacers, and spiral type pipes inside the SG. A hybrid meshing technique was used with inflated boundaries mainly at the core rods and the SG tubes, with a spacing of 0.01 mm for the wall closest layer in order to obtain $y+$ values close to 1. For saving cells, and because of the adiabatic boundary condition at the outer vessel wall in the downcomer, larger values of 0.1 mm are used. The grid, which was created by using the Pointwise meshing software by Cadence,[1] contains about $2 \cdot 10^8$ cells at a maximum cell size of about 20 mm.

In order to find an explanation for some temperature deviations in the SG downcomer region, a standalone model for the SG was created (see Fig. 10). On the primary side, the meshing technique is similar as described above for the entire facility model, while on the secondary side, the fluid region inside the spiral tubes is meshed without additional refinement. In this model, the full SG piping system was considered with additional ring pipe collectors at the SG inlet and outlet, together with multiphase flow on the secondary side inside the spiral pipes. Additionally, thermocouple positions in this facility area (T6004-6013, red crosses) are shown in Fig. 10.

All simulations were performed as RANS steady-state simulations by using an ω-Reynolds Stress turbulence model (Clarke and Wilkes, 1989). Because the primary flow is driven only by density differences in the core, a buoyancy model was applied. Furthermore, for the calculation of turbulent heat transfer, a standard Reynolds analogy was applied by using a turbulent Prandtl number of 0.9. For numerical discretization, a higher order method with a blending procedure between 1st order in regions with strong gradients and 2nd order otherwise was used.

The primary coolant was considered as liquid water with temperature and pressure dependent properties as provided by the IAPWS tables.[2] Conjugate heat transfer is applied for the heater rod claddings and the solid parts of the measurement rods in the core, the wall that separates the downcomer from the core and the riser region, and for the SG pipes. All those components are considered as steel with a temperature independent thermal conductivity of 15 W/m^2/K. In the SG standalone model, the coolant is treated as a binary homogeneous water–steam mixture with transition between the phases, see ANSYS (2024).

CFX standard convergence conditions for RMS residuals, together with a conservation target, were used. It has to be mentioned that a full convergence could not be reached because of instabilities of the natural convection flow. RMS residuals reached only values of

[1] https://www.pointwise.com

[2] The International Association for the Properties of Water and Steam: http://www.iapws.org.

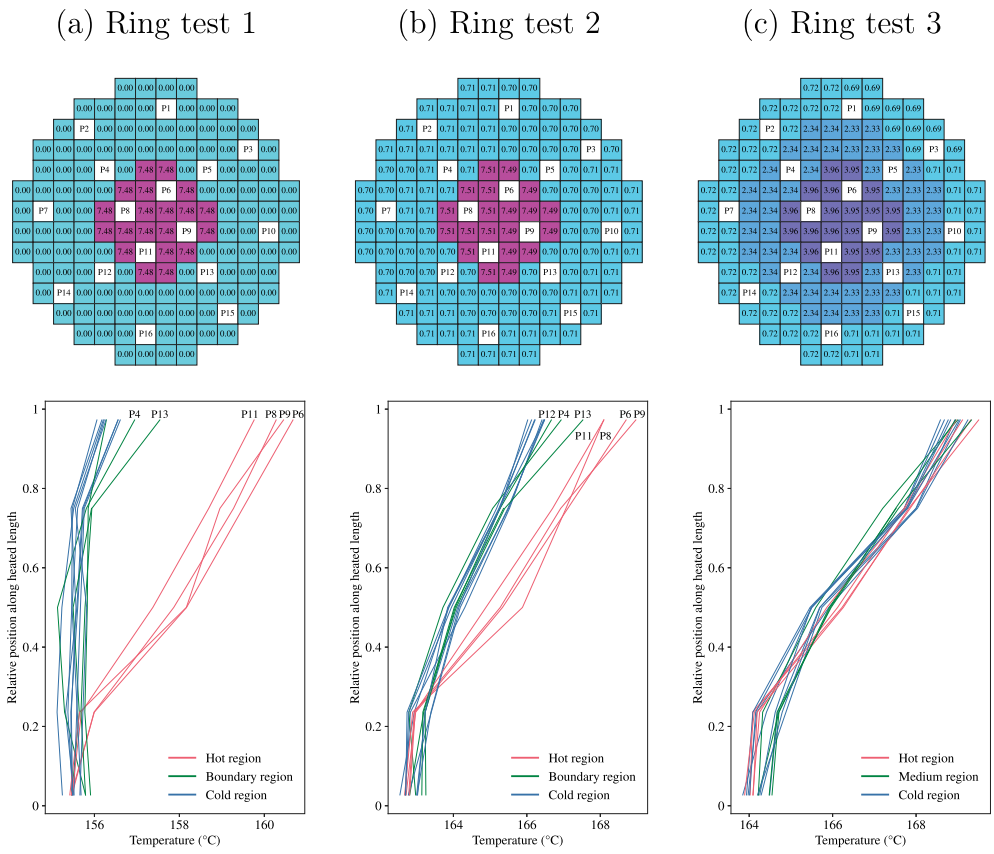

Fig. 8. Axial fluid temperature profiles measured with the instrument probes in three ring-shaped heating power tests. The curves are coloured based on their location, either in the region with the highest heating power (Hot region), the unheated or lower heating power region (Cold region), or in the cold region but right next to the hot region (Boundary region). In Ring test 3, with three different power regions, the region in between the hot and cold regions is termed as the Medium region. The applied power distribution in each test is displayed above, with the numbers being the power of each heater rod in kW.

about $2 \cdot 10^{-4}$, while values equal or below 10^{-4} can be considered as converged. Additionally, temperatures at monitor points in the core region were oscillating by ±0.1 K. A similar behaviour was observed in the experiments, where ideal steady state conditions could not be obtained.

For the CFD model, which considers the complete vessel, the outer vessel wall is treated as adiabatic. An absolute pressure of 20 bar in the centre of the vessel is assumed. In case of steady state conditions, the total heater power P_{core} has to be removed by the SG. In order to provide a temperature reference point for steady state conditions for the solver, the heat removal by the SGs, which are modelled by the helical coil SG pipes, is specified as temperature dependent heat flux boundary condition at the SG pipes as

$$Q_{\text{SG}} = -\frac{P_{\text{core}}}{A_{\text{SG}}} \frac{T_{\text{SG,out}} - T_1}{T_2 - T_1}, \tag{1}$$

with $T_1 = 145.4$ °C, $T_2 - T_1 = 21$ °C, $P_{\text{core}} = 230$ kW dependent on the scenario, and the SG area $A_{\text{SG}} = 17.0$ m^2. $T_{\text{SG,out}}$ is a mass flow averaged temperature for the cross section of the downcomer below the SG, while T_1 and T_2 are derived from measured temperatures.

4.2. CFD results

Fig. 11 shows the temperature and velocity distribution inside the vessel. The asymmetric buoyancy force inside the core generates an uprising jet, which becomes unstable when leaving the heated core section. Some recirculation zones are formed, and the flow in the core region and above is very inhomogeneous. There is also a feedback between the flow in the downcomer and the flow leaving the core in upward direction, triggered by conjugate heat transfer through the separating wall. The flow asymmetry at the core outlet penetrates into the SGs, and finally, the velocity distribution at the lower core entrance remains asymmetric, while the temperature at the core inlet is closer to homogeneous conditions.

The velocity distribution at the lower axial position, where the downcomer ends and the coolant enters into the lower plenum towards the core, is presented within Fig. 11. While the temperature differences in the downcomer gap are lower than 0.6 °C, the axial velocity distribution in the gap is significantly asymmetric. As consequence, this asymmetry also propagates into the asymmetric heated core and makes simulations for system tools with significantly coarser spatial resolutions challenging.

In Fig. 12, a comparison of temperatures at selected positions of thermocouples in the core region is presented. The designation “Height” means the distance from the bottom of the vessel. The locations of the probes in the core map can be seen in Fig. 4, and they have been selected to represent the different core regions of this asymmetric heating case. At all positions, a good agreement between the measured data and the simulation can be observed, with absolute differences < 1 °C, which is below the specified measurement accuracy of ±2 °C. The positions P2 and P8 are located in a heated section, while position P6 is neighboured with a heated section but itself unheated. Position P10 has a maximum distance of all measurement rods to the heated sections. Because of crossflow, mainly in the upper part of the core, coolant from heated parts is mixed into unheated regions. This transport seems to be supported by natural convection, which is forming recirculation regions in the core between heated and unheated parts.

Furthermore, the massflow in the downcomer is in very good agreement with the experimental data. The experimental value of 9.09 kg/s was slightly underestimated by about 3 % to 8.8 kg/s.

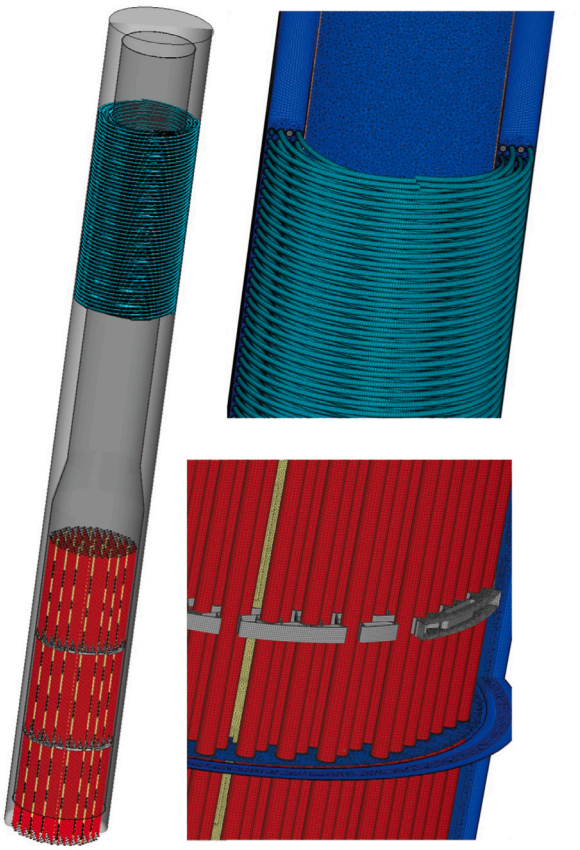

Fig. 9. The CFD model with meshing details of the SG and the core.

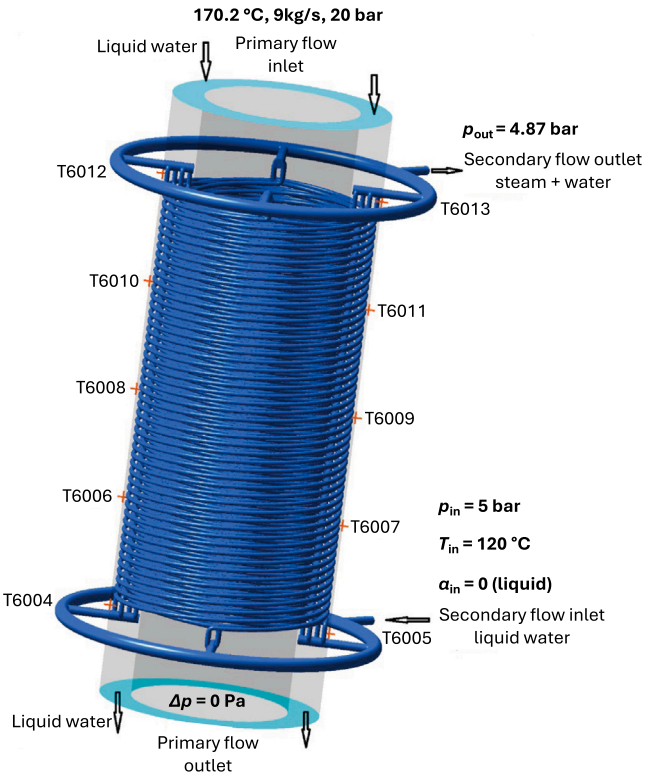

Fig. 10. Configuration of the standalone SG model as a heat flux boundary condition for the core heater rods.

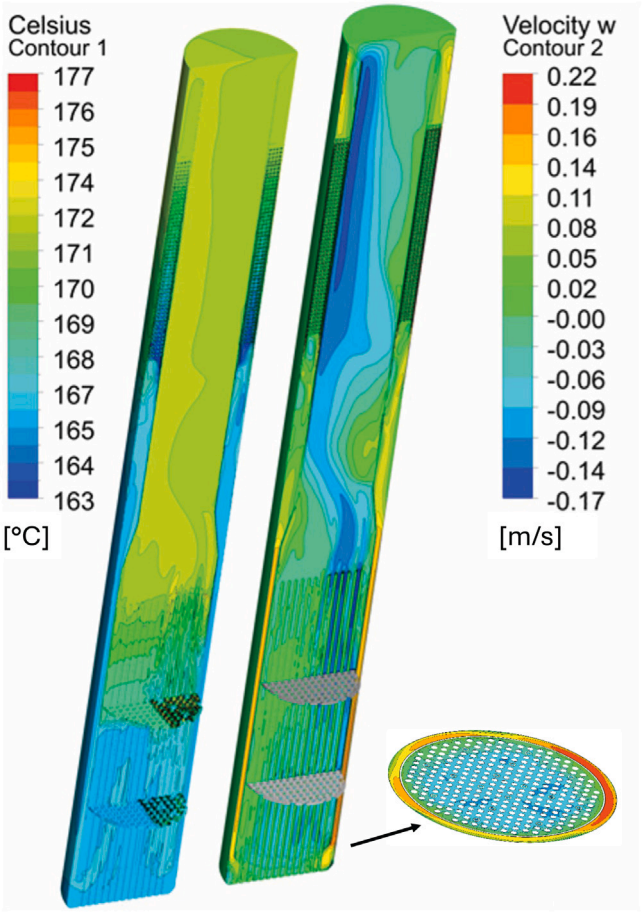

Fig. 11. Temperature and velocity distribution.

Fig. 13 presents a similar comparison of temperatures at downcomer positions in the SG region for the model covering the full vessel (turquoise curves) and for the SG standalone model. The thermocouple positions are indicated within Fig. 10. The boundary conditions, also listed in Fig. 10, are derived from the CFD facility model on the primary side and from measurements on the secondary side. At an inlet pressure of 5 bar and at 120 °C on the secondary side, the water enters as liquid and evaporates quickly. At the secondary side outlet, nearly pure steam is leaving. It has to be mentioned that absolute pressures of 5 bar at the inlet and 4.87 bar at the outlet were used as boundary conditions.

Mainly at the location of the SG, locally some larger deviations up to 4 °C are calculated by the CFD facility model. The measured temperatures are overestimated, but at the entrance and below the SG region, the differences against measured data are approaching about 0.5 °C. The reason for larger differences inside the SG region is the simplified heat removal model, which uses a spatially constant heat flux at SG tube surfaces. The spiral type SG in counter flow orientation of primary and secondary flow has significantly better heat transfer conditions in its vertical lower part, because here the coolant at the secondary side enters as liquid and leaves the SG as liquid/steam mixture, which means a deterioration of heat transfer conditions at the secondary side. As consequence, some improvement is obtained by implementation of the multiphase flow on the secondary side. The deviations against measurements (red curves) are now less than 1.5 °C. It has to be mentioned, that overall average deviation between calculated temperature and thermocouple data is about 0.2 K. The reason therefore maybe the neglection of thermal losses at the outer boundaries, which are considered as adiabatic.

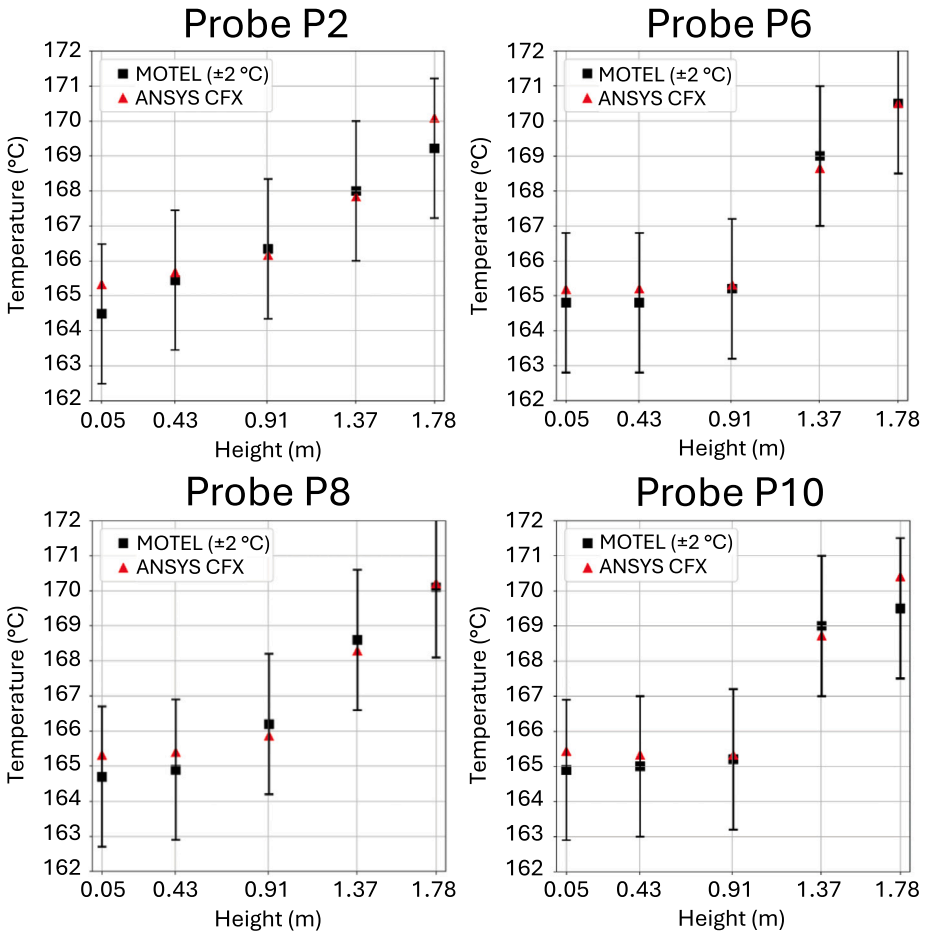

Fig. 12. Temperatures at selected measurement rod positions in the core region.

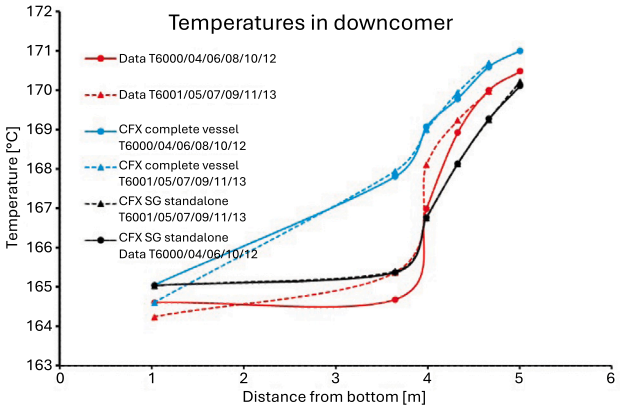

Fig. 13. Temperatures in downcomer at SG position.

5. Subchannel code simulations

The data obtained from the MOTEL experiments was used for the validation of two subchannel codes, namely CTF and VIPRE-01. These represent thermal-hydraulic analysis tools developed specifically for the reactor core simulations to predict safety relevant parameters, such as the minimum departure from nucleate boiling ratios (MDNBR) and fuel and cladding maximum temperatures. Section 5.1 provides the description of the CTF simulation model and results, while Section 5.2 discusses the VIPRE-01 simulations.

5.1. CTF simulations

CTF is a subchannel thermal-hydraulic software for light water reactors modelling, initially developed by the Pacific Northwest National Laboratory (PNNL) (Salko et al., 2020). It is presently maintained by the North Carolina State University (NCSU) and Oak Ridge National Laboratory (ORNL). CTF models the coolant flow behaviour, heat transfer, and coolant interaction with the reactor structures, including fuel rods, grids, and the vessel. The code employs a two-fluid (liquid and vapour)–three-field (liquid bulk, dispersed liquid, vapour) modelling approach.

Initially, CTF was primarily used to model conventional Pressurized Water Reactors (PWRs) and Boiling Water Reactors (BWRs) under forced convection conditions. However, with the emergence of reactor designs that rely on natural circulation during accidental scenarios and/or normal operation, the code's capabilities have been extended. Specifically, it now accounts for lower mass flow rates. These developments have been validated with experimental data from the PNNL 2x6 rod bundle facility (Blyth et al., 2015). The MOTEL crossflow experiments serve as an additional and valuable database to evaluate CTF's performance under natural circulation conditions. CTF's model and simulation results of the experiments presented in Section 3 are described in the subsequent paragraphs.

5.1.1. CTF model

CTF models the MOTEL core using 148 subchannels, centred around the heated and measurement rods, as shown in Fig. 14. Each rod is represented by a "solid conductor" structure with 8 radial nodes within the rod and 23 axial nodes. Subchannels are divided into 23 axial

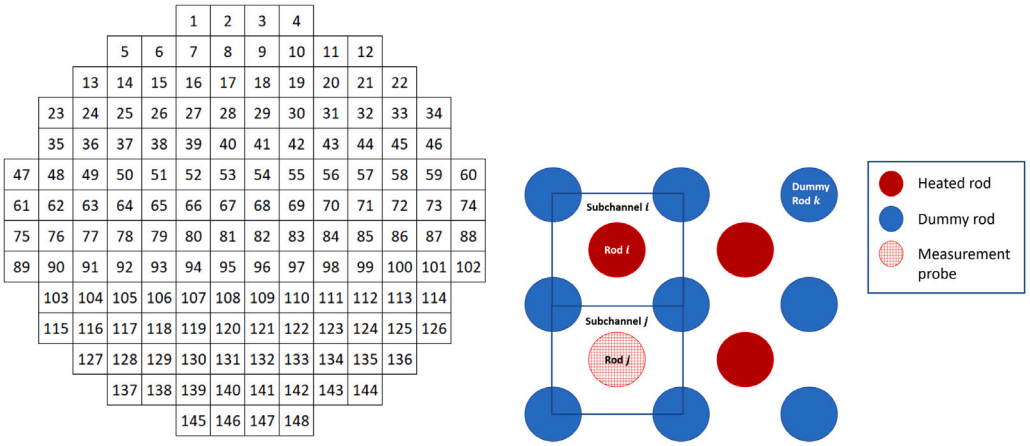

Fig. 14. Subchannel and rod numbering (top), and the CTF subchannel definition (bottom).

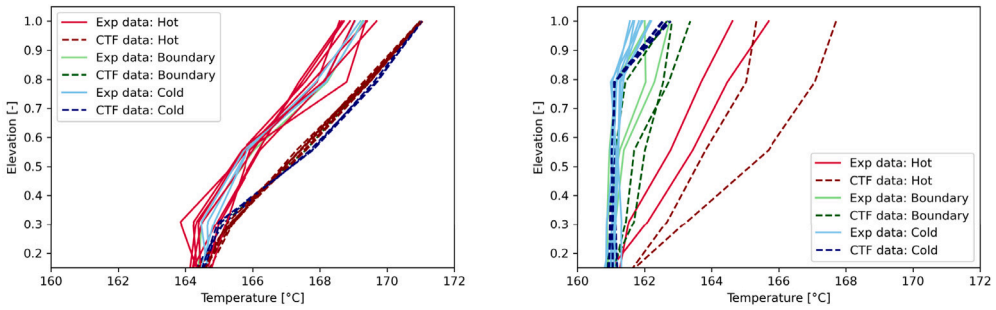

Fig. 15. Asymmetric tests: Temperature evolution over normalized axial location for test 2 (left) and test 4 (right). Experimental results are plotted in solid lines, and CTF results in dashed lines.

cells. Two support plates are positioned at axial elevations 660 mm and 1320 mm (axial cells 8 and 16, respectively). A total of 268 gaps allow modelling of crossflows between adjacent subchannels.

CTF models the effect of the support plate on the flow by applying a local pressure loss in axial cells 8 and 16 at axial elevations 660 mm and 1320 mm, respectively. To account for friction, the model uses the original CTF correlation of the rod friction factor λ (Salko et al., 2020) that reads:

$$\lambda = \max\left(1.691 Re^{-0.43}, 0.117 Re^{-0.14}\right), \tag{2}$$

where Re is the Reynolds number. The single-phase turbulent mixing coefficient remains constant at $\beta = 0.05$. Electrically heated rods act as heated conductors, meaning that heat is generated within the conductor volume. Measurement and dummy rods conduct heat but do not generate heat themselves. Both axial and radial conduction effects are considered in the model.

Two CTF simulations were conducted with initial and boundary conditions based on experimental measurements plotted in Figs. 5 and 6. A moving average of experimental data was used to avoid convergence issues due to measurement noise. The core outlet pressure was set at 20 bar.

5.1.2. CTF results

Temperature axial profiles of tests 2 and 4 of the asymmetric series are plotted in Fig. 15, and tests 1 and 3 of the ring series are plotted in Fig. 16. The figures show that CTF captures the correct trend for all subchannel types. For instance, CTF reproduces the clear distinctive trend between profiles depending on the zone where they are located (hot/boundary/cold) in test 4 of the asymmetric series and test 1 of the ring series. These results show that CTF is in good agreement with experimental data, although the code overestimates the temperature for all subchannel types.

This is confirmed in Figs. 17 and 18, where experimental and CTF numerical temperature profiles are plotted over time in two subchannels containing probes P2 (hot zone) and P13 (cold zone) for the asymmetric tests and P8 (hot zone) and P3 (cold zone) for the ring tests. The figures show that numerical results are in good agreement with experimental data for lower elevations upstream the lower support plate ($x = 0.22$ m). Downstream the support plate, CTF predicts temperatures between 1 °C to 4 °C higher than experiments. The highest difference is ~ 4 °C at the elevation $x = 1.085$ m, located between the two support plates.

Results highlight the capacity of CTF to predict the proper trend for all subchannel types, numerical data being in fair agreement with the experiments. The agreement with experimental data is excellent for lower elevations upstream the lower support plate, and decreases downstream.

5.2. VIPRE-01 simulations

VIPRE-01 is an American subchannel analysis code used for the thermal-hydraulic analysis of reactor cores or similar geometries under both steady-state and transient conditions (Battelle, 2020). The program is generally intended for analyses of both PWRs and BWRs. Detailed thermal-hydraulic parameters of fuel and coolant can be calculated by VIPRE-01, including temperature, pressure, mass flux, and quality. A significant application of VIPRE-01 is the determination of the MDNBR to evaluate whether a boiling crisis occurs under specific conditions.

5.2.1. VIPRE-01 model

The model of the MOTEL facility in the VIPRE-01 code consists of 328 subchannels. These are defined by the lines drawn through the centre of adjacent rods, as illustrated in Fig. 19. The heated length is

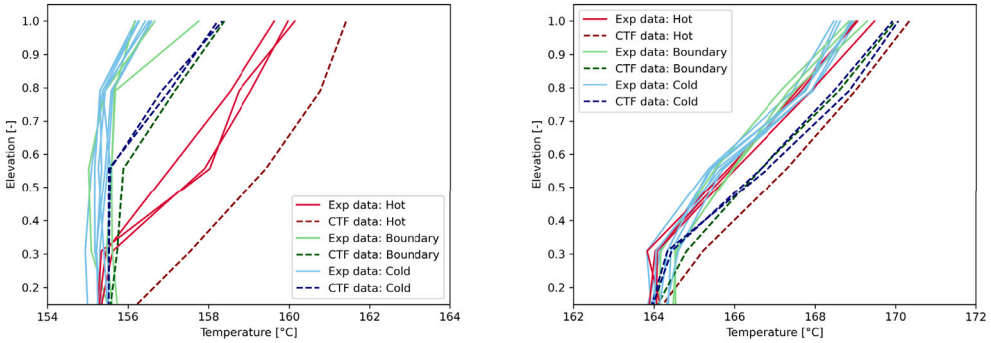

Fig. 16. Ring tests: Temperature evolution over normalized axial location for test 1 (left) and test 3 (right). Experimental results are plotted in solid lines, and CTF results in dashed lines.

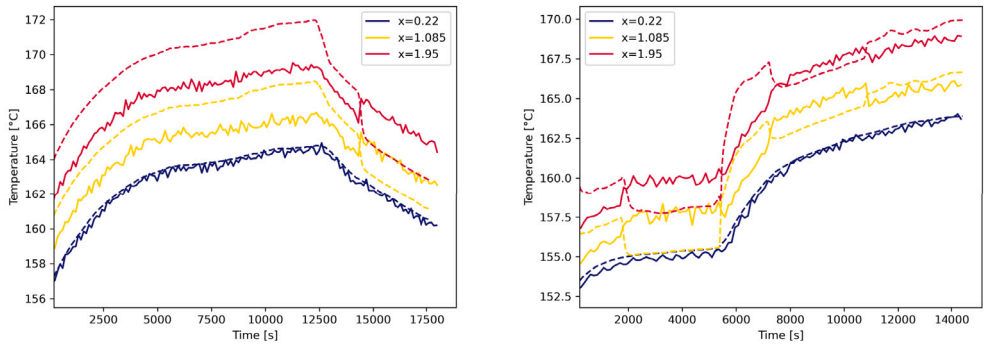

Fig. 17. Temperature evolution over time at different elevations in a hot channel for asymmetric (left, results at probe P2) and ring (right, results at probe P8) experiments. Experimental results are plotted in solid lines, and CTF results in dashed lines.

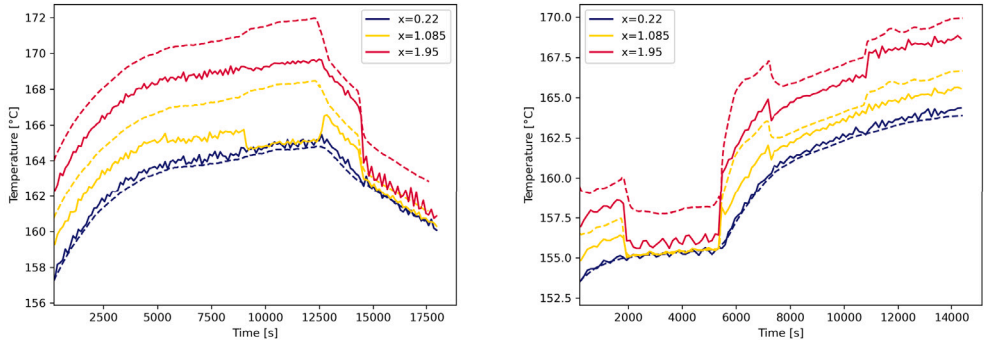

Fig. 18. Temperature evolution over time at different elevations in a cold channel for asymmetric (left, results at probe P13) and ring (right, results at probe P3) experiments. Experimental results are plotted in solid lines, and CTF results in dashed lines.

axially divided into 240 equal nodes. The total number of gaps between subchannels is 620.

5.2.2. VIPRE-01 results

It was found that the boundary conditions of the MOTEL experiments are beyond the conditions which can be simulated by the VIPRE-01 code. The reference runs with powers of 150 kW and 230 kW were calculated first, but despite the efforts made, all of the calculations eventually diverged. Improvement in numerical stability was observed in the case of higher axial nodalization when the number of axial nodes along the heated length was gradually increased from 62 to 240. However, the mass flow rate in the experiments was too low to successfully complete the calculations. When the mass flow rate was experimentally defined as four times higher in the input-deck to investigate the capacity of VIPRE-01 to handle more favourable conditions, the calculation ended successfully. By performing a sensitivity analysis, it was found that the lowest value of the coolant mass flow rate for which the solution converges is 18.2 kg/s and 21.2 kg/s for the reference runs of 150 kW and 235 kW, respectively, while the other experimental conditions remain unchanged in the analyses. The precision of the determined mass flow rate boundary values is 0.1 kg/s. As can be seen from Fig. 6, the coolant mass flow rate boundary values are several times higher than the mass flow rate values measured in the experiments. The other runs with non-uniform radial power distribution were not able to be computed because of the excessively high average rod power.

6. Conclusions

An effort to generate new measurement data relevant for light-water SMRs and subsequently validate thermal hydraulic safety analysis tools was realized within the European McSAFER project. This paper presented one set of experiments and validation activities focused on the natural circulation driven core flow and heat transfer phenomena in

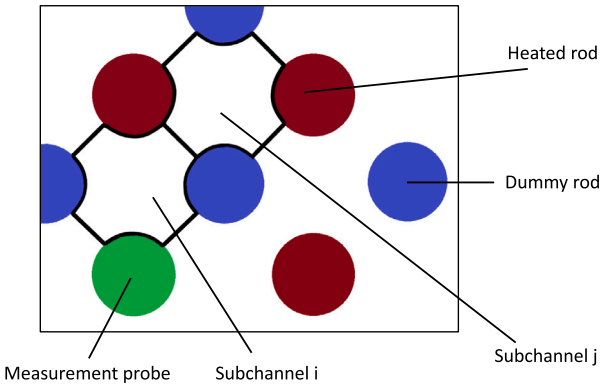

Fig. 19. Definition of subchannels in the VIPRE-01 model of the MOTEL facility.

an iPWR type configuration. The experiments were conducted with the MOTEL test facility and consisted of experiments with asymmetric and ring-shaped core heating profiles. Fluid temperature in the core was measured with thermocouples installed into hollow measurement rods, and two ultrasonic flowmeters provided an estimate for the core flow rate. CFD simulations for one of the asymmetric tests were performed with a CFD model resolving the entire primary side in detail. Further CFD investigations were performed with a stand-alone model of the steam generator, in which also the two-phase flow and heat transfer in the secondary side was considered. Subchannel simulations of the MOTEL experiments were performed with the codes CTF and VIPRE-01, of which the CTF simulations were successfully completed for all test cases, while the VIPRE-01 simulations suffered from convergence issues and ended unsuccessfully.

The main conclusions and experience from the experiments are the following.

- Relatively high power gradients between the heater sections are required before notable differences between the thermocouple measurements across the core cross section are seen. With high enough power gradients, the temperature curves in the heated sections start to deviate from those in the unheated or lower power region.
- Based on the temperature measurements, cross flow mixing occurs mainly in the top part of the core and most visibly in the asymmetric tests. This is seen either as increased temperatures in the probe locations at the boundary of the "hot" and "cold" regions, or as nearly homogeneous outlet temperatures in all probe locations following an initial separation to warmer and colder streams in the lower part of the core.
- The capabilities of the MOTEL facility for core heating experiments with radial power gradients was demonstrated, and it can be used for further tests either as such, or thanks to its modular design, after replacing the core or the heat exchanger to some other design.

The experiments with the MOTEL facility featured an integral PWR configuration with buoyancy induced low-velocity flow in the primary side, together with asymmetric heating up to relatively sharp gradients between heater sections. These characteristics make the experiments challenging cases for simulation tools.

The main conclusions and experience from the CFD simulations are the following.

- The presented CFD model for the entire MOTEL vessel shows good agreement with experimental data, even at low power level, and in case of asymmetric core heating. A key point is the full resolution of structures with impact on the pressure loss.
- A local model improvement could be obtained by the implementation of two-phase flow on the secondary side of the SG, as shown in the standalone SG study. Because of convergence problems, the implementation of two-phase flow on the secondary side appears to be problematic in a CFD model for the entire vessel. As consequence, an implementation of axial and temperature dependent heat flux profiles, derived from the results of the SG standalone model in the facility model, could be an option for further model improvement.

The main conclusions and experience from the subchannel simulations are the following.

- CTF results are in fair agreement with experimental data, with the highest difference being around 4 °C.
- CTF is able to predict the correct trend, with excellent agreement for lower elevations, and good to fair agreement for higher elevations, especially compared to the measurements uncertainties (±2 °C).
- CTF results clearly highlight its capacity to handle pressure and velocities typical of natural circulation driven light water SMR reactor designs. Given that the temperature is overestimated by CTF for all subchannel types, including those located in the cold zone, the discrepancies with experimental data are not attributed to the mixing being underestimated in CTF. On the contrary, results show that the code has a good capacity to model mixing by computing the correct crossflows. Instead, the overestimation of temperature could be related to losses to the environment being neglected in CTF calculations.
- It was found that the solution and its stability in the VIPRE-01 code are highly sensitive to mass flow rate, power level, and axial nodalization.
- With convergence issues in all attempted simulations with VIPRE-01, the boundary conditions of the MOTEL experiments are concluded to be beyond the conditions that can be simulated by the VIPRE-01 code.

CRediT authorship contribution statement

Heikki Suikkanen: Writing – original draft, Visualization, Project administration, Investigation, Funding acquisition, Formal analysis, Data curation, Conceptualization. **Joonas Telkkä:** Writing – original draft, Supervision, Methodology, Investigation, Formal analysis. **Antti Räsänen:** Methodology, Investigation. **Eetu Kotro:** Methodology, Investigation. **Michael Böttcher:** Writing – original draft, Visualization, Validation, Methodology, Investigation, Formal analysis, Data curation, Conceptualization. **Lucia Rueda-Villegas:** Writing – original draft, Visualization, Validation, Methodology, Investigation, Formal analysis, Data curation, Conceptualization. **Veronika Sunkova:** Writing – original draft, Visualization, Validation, Methodology, Investigation, Formal analysis, Data curation, Conceptualization.

Declaration of Generative AI and AI-assisted technologies in the writing process

During the preparation of this work the author(s) used Microsoft Copilot in order to check punctuation in the text. After using this tool/service, the author(s) reviewed and edited the content as needed and take(s) full responsibility for the content of the publication.

Declaration of competing interest

The authors declare the following financial interests/personal relationships which may be considered as potential competing interests: Heikki Suikkanen reports financial support was provided by European Commission. Joonas Telkka reports financial support was provided by European Commission. Antti Rasanen reports financial support was

provided by European Commission. Eetu Kotro reports financial support was provided by European Commission. Michael Bottcher reports financial support was provided by European Commission. Lucia Rueda-Villegas reports financial support was provided by European Commission. Veronika Sunkova reports financial support was provided by European Commission. If there are other authors, they declare that they have no known competing financial interests or personal relationships that could have appeared to influence the work reported in this paper.

Acknowledgements

This project has received funding from the Euratom research and training programme 2019–2020 under grant agreement No 945063. The content of this paper reflects only the authors' views and the European Commission is not responsible for any use that may be made of the information it contains.

Data availability

The authors do not have permission to share data.

References

Al-Othman, A., Darwish, N.N., Qasim, M., Tawalbeh, M., Darwish, N.A., Hilal, N., 2019. Nuclear desalination: A state-of-the-art review. Desalination 457, 39–61. http://dx.doi.org/10.1016/j.desal.2019.01.002.

ANSYS, 2024. ANSYS CFX-Pre User's Guide. ANSYS, Inc.

Battelle, 2020. VIPRE-01: A Thermal-Hydraulic Code for Reactor Cores, Volume 1: Mathematical Modeling, Revision 5. Battelle, Pacific Northwest Laboratories, Zachry Nuclear Engineering, Inc., EPRI.

Blyth, T., Dances, C., Avramova, M., Salko, R., 2015. CTF validation activities. In: Proceedings of the 16th International Topical Meeting on Nuclear Reactor Thermal Hydraulics. NURETH-16, pp. 7154–7167.

Clarke, D.S., Wilkes, N.S., 1989. The Calculation of Turbulent Flows in Complex Geometries Using a Differential Stress Model. AERE-R 13428, Harwell Laboratory, United Kingdom Atomic Energy Authority.

Hyvärinen, J., Riikonen, V., Telkkä, J., Hujala, E., Kouhia, V., Puustinen, M., Patel, G., Pyy, L., Vihavainen, J., Suikkanen, H., Rintala, V., 2024. Creating the foundations for safe nuclear power in Finland – Thermal hydraulics, safety analyses, safety justification methods research at the LUT University, 2000–2023. Nucl. Eng. Des. 419, 112935. http://dx.doi.org/10.1016/j.nucengdes.2024.112935.

Hyvärinen, J., Telkkä, J., Kauppinen, O., Purhonen, H., 2017. MOTEL – modular design and physical scaling principles of the next generation thermal hydraulics test facility at LUT. In: Proceedings of the 17th International Topical Meeting on Nuclear Reactor Thermal Hydraulics. NURETH-17, Xi'an, China, September 3–8, 2017, pp. 5128–5141.

Hyvärinen, J., Telkkä, J., Tielinen, K., 2022. MOTEL-SMR integral PWR system test facility - design and first test results. In: Proceedings of the 19th International Topical Meeting on Nuclear Reactor Thermal Hydraulics. NURETH-19, Virtual Meeting, March 7–11, 2022, p. 35551.

IAEA, 2019. Deterministic Safety Analysis for Nuclear Power Plants, Specific Safety Guide. IAEA Safety Standards Series No. SSG-2 (Rev. 1), International Atomic Energy Agency.

IAEA, 2022. Advances in Small Modular Reactor Technology Developments, 2022 Edition. A Supplement to: IAEA Advanced Reactors Information System (ARIS). International Atomic Energy Agency.

Ingersoll, D., Houghton, Z., Bromm, R., Desportes, C., 2014. NuScale small modular reactor for co-generation of electricity and water. Desalination 340, 84–93. http://dx.doi.org/10.1016/j.desal.2014.02.023.

Leppänen, J., Hillberg, S., Hovi, V., Komu, R., Kurki, J., Lauranto, U., Oinonen, A., Peltonen, J., Rintala, A., Tulkki, V., Tuominen, R., Valtavirta, V., 2021. A Finnish district heating reactor: Background and general overview. In: Proceedings of the 2021 28th International Conference on Nuclear Engineering. Volume 1: Operating Plant Challenges, Successes, and Lessons Learned; Nuclear Plant Engineering; Advanced Reactors and Fusion; Small Modular and Micro-Reactors Technologies and Applications. Virtual, Online. August 4–6, 2021, ASME, V001T04A009. http://dx.doi.org/10.1115/ICONE28-64346.

Lloyd, C.A., Roulstone, T., Lyons, R.E., 2021. Transport, constructability, and economic advantages of SMR modularization. Prog. Nucl. Energy 134, 103672. http://dx.doi.org/10.1016/j.pnucene.2021.103672.

Locatelli, G., Boarin, S., Fiordaliso, A., Ricotti, M.E., 2018. Load following of Small Modular Reactors (SMR) by cogeneration of hydrogen: A techno-economic analysis. Energy 148, 494–505. http://dx.doi.org/10.1016/j.energy.2018.01.041.

Mignacca, B., Locatelli, G., 2020. Economics and finance of Small Modular Reactors: A systematic review and research agenda. Renew. Sustain. Energy Rev. 118, 109519. http://dx.doi.org/10.1016/j.rser.2019.109519.

Peakman, A., Merk, B., 2019. The role of nuclear power in meeting current and future industrial process heat demands. Energies 12 (19), 3664. http://dx.doi.org/10.3390/en12193664.

Salko, R., Avramova, M., Wysocki, A., Toptan, A., Hu, J., Porter, N., Blyth, T., Dances, C., Gomez, A., Jernigan, C., Kelly, J., Abarca, A., 2020. CTF Theory Manual. North Carolina State University.

Sanchez-Espinoza, V.H., Gabriel, S., Suikkanen, H., Telkkä, J., Valtavirta, V., Bencik, M., Kliem, S., Queral, C., Farda, A., Abéguilé, F., Smith, P., Uffelen, P.V., Ammirabile, L., Seidl, M., Schneidesch, C., Grishchenko, D., Lestani, H., 2021. The H2020 McSAFER project: Main goals, technical work program, and status. Energies 14 (19), 6348. http://dx.doi.org/10.3390/en14196348.

Skoda, R., Fortova, A., Masata, D., Zavorka, J., Lovecky, M., Skarohlid, J., Kolar, F., Vilimova, E., Peltan, T., Burian, O., Jirickova, J., 2020. TEPLATOR: Nuclear district heating solution. In: Proceedings of the International Conference Nuclear Energy for New Europe. NENE2020, Portoroz, Slovenia, September 7–10, 2020, p. 408.

Suikkanen, H., Telkkä, J., Kouhia, V., Gabriel, S., Heiler, W., Heineken, F., Sanchez-Espinoza, V., Li, H., Grishchenko, D., Bencik, M., Vyskocil, L., Queral, C., Fernandez-Cosials, K., Rueda-Villegas, L., Schneidesch, C., 2023. Thermal hydraulic experiments and code validation for LWR SMRs within the European McSAFER project: Overview of activities and current status. In: Proceedings of the 20th International Topical Meeting on Nuclear Reactor Thermal Hydraulics. NURETH-20, pp. 2388–2401.

Telkkä, J., Suikkanen, H., Räsänen, A., Kotro, E., Hyvärinen, J., 2023. Helical coil steam generator experiments with the MOTEL SMR test facility in the EU-McSAFER project. In: Proceedings of the 20th International Topical Meeting on Nuclear Reactor Thermal Hydraulics. NURETH-20, pp. 1662–1675.

Truong, T., Suikkanen, H., Hyvärinen, J., 2021. Reactor core conceptual design for a scalable heating experimental reactor, LUTHER. J. Nucl. Eng. 2 (2), 207–214. http://dx.doi.org/10.3390/jne2020019.